Analysis of Thermal Video for Coarse to Fine Particle Tracking in Volcanic Explosion Plumes

Maxime Bombrun, Vincent Barra, Andrew Harris

Analysis of thermal video for coarse to fine particles tracking in volcanic explosion plumes

Maxime Bombrun,[1,2,3,4] Vincent Barra,[1,2] Andrew Harris,[3,4]

[1] Clermont-Université, Université Blaise Pascal, LIMOS, BP 10448, F-63000 CLERMONT-FDERRAND, France
[2] CNRS, UMR 6158, LIMOS, F-63173 AUBIERE, France
[3] Clermont-Université, Université Blaise Pascal, LMV, BP 10448, F-63000 CLERMONT-FERRAND, France
[4] CNRS, UMR 6524, LMV, F-63038 CLERMONT-FERRAND, France

Abstract. This paper presents two algorithms of feature extraction and segmentation. The first algorithm is applied to detect tens of thousands of targets moving at high velocities (100's m/s) and with different sizes, velocities, shapes and directions. Upon detection, we compute statistics for each of these parameters for each particle, without any assumption nor a priori information. The second algorithm was developed to detect a slow moving convective cloud. The challenge was to follow the evolution of the contours of a heterogeneous element in front of a homogeneous but possibly moving background. These algorithms were applied on images acquired with thermal cameras with different settings (frame rate, frame size, focal length, instantaneous field of view). A case study concerning images of volcanic explosive events is finally presented. Volcanoes provide, during an eruption, a source of both ballistic ejecta and a convective plume of finer particles, gas and entrained air both of which can be imaged in the infrared wavelength. **: Results ?**

Keywords: segmentation; feature extraction; contours; thermal imagery

Introduction

The first infrared high-temporal-resolution system, operating at 20 images per second, was produced in 1965. However, the first hand-held system came with the introduction of high-spatial resolution focal plane arrays in 1993, and the first uncooled micro-bolometer-based system was produced in 1997. These developments, coupled with evolutions in high-speed digital electronics that allowed imagery to be stored on small memory disks "revolutionized the commercialization of thermal imaging systems" [Holst, 2000]. From here onwards, infrared imaging science expanded rapidly in many domains [Kylili et al., 2014]. Thermal imaging cameras (TIC) produce a thermal image of a scene that provides information about both its temperature and radiative properties. Thus, TIC can be selected to be useful in multitude of hot spot tracking roles.
Infrared Search and Track (IRST) systems were first developed for air defence

applications [Jong, 1995]. Today, they are also used in civil applications, such as surveillance on land, at sea and in the air and warning against intruders [Fernandez-Caballero et al., 2011], survey danger areas where disasters may occur. IRST is also used in military applications. Thermal emission of gears operating on tanks or helicopters can, for example, be used to detect, track and lock-on to the target, so that many automatic target recognition (ATR) algorithms have been proposed [Li et al., 2001]. These segment and recognize vehicles, ships and aircrafts [e.g. Yilmaz et al., 2003]. TIC can be selected in a wide range of applications, including fire control [Amon and Pearson, 2009], monitoring of buildings [Kylili et al., 2014], medicine [Arora et al., 2008] and computer-aided diagnosis systems [Faust et al., 2014] or volcanology. In this case, one of the first field-based thermal measurement campaigns at an active volcano was completed by Thomas A. Jaggar [1917a,b]. He illustrated the benefits of remote thermal measurements against the common contact measurements, describing problems including equipment and personnel safety, and the limited measurement time available for a contact measurement imposed by the radiated heat from a lava lake. The first attempt to run a radiometer continuously was completed for a persistent degassing by Tazieff [1970] and during an explosive event by Shimozuru [1971]. Between 1965 and the end of 2007, at least 60 studies reported results obtained using ground-based broad-band radiometers for explosions, fumaroles and geothermally heated surfaces as well as lava flow, lakes and domes [Harris, 2013]. These applications of volcanological science achieved using thermal cameras were clustered in five main groups by Spampinato et al. [2011]: hydrothermal areas and fumarole fields; lava bodies; explosive activity and volcanic plumes; pyroclastic flow deposits; fracturing and cracking. The most popular being the explosive activity (which accounted for 48 % of the studies published between 2001 and 2011). The key advance has been the ability to collect thermal video with spatial resolutions of a few centimeters and sampling frequencies of up to 120 Hz, with the operator being free to choose and modify the dynamic range, sampling rate, field of view, and targeted area, as well as acquisition start and stop times. Some of the first progress in the domain of volcanology to made were applications to track the dynamics of strombolian eruption plumes [Dehn et al., 2001].

In this paper, we aim to segment two major components of an explosive volcanic eruption using thermal video. First, we focused on all coarse particles as they exit the vent to gather parameters such as size, shape, velocity and mass for the solid (particulate) fraction of the plume, this being the contribution of particles with a diameter between 1 cm and 5 cm (lapilli-size) and between 6.5 cm to 35 cm (bombs-sized). We then analyzed the plume of gas and fine particles whose ascent will be buoyancy driven [Turner, 1962] and which can rise 100 meters up to over 25 000 meters above the vent. Thermal cameras have been used for plume tracking [Spampinato et al., 2011; Valade et al., 2014], however, the changing contrast between the optical properties of the emission and the background, and the evolution of plume properties over long time periods imply that the segmentation of volcanic plume remain a challenge.

1 Particle study (cm-sized analysis)

1.1 Methodology

The thermal camera used in this study was a forward looking infrared (FLIR). We used a FLIR Systems SC655, equipped with a 3.6× magnification lens and recording at 200 frames per second. The focal length was 88.9 mm and the IFOV was 0.19 mrad. Our acquisition frequency. We note that our frames usually have a size 600 × 480 pixels, but are automatically truncated to allow recording at rates greater than 30 Hz; for example, at 200 Hz, the image size is 600 × 120 pixels. This resizing is automatically performed by the acquisition software and the resized frame is centered on the same pixel as the large frame and the spatial resolution does not change. The spatial resolution (or pixel dimension, L_p) will depend on the detector instantaneous field of view (IFOV), which is defined by a cone opening at angle β_{IFOV}, and the distance to the target (D), so that the pixel diameter is given by $L_p = 2[Dtan(\beta_{IFOV}/2)] = D \times \beta_{IFOV}$, using paraxial approximation defined for the small angle.

Given the large number of particles expected and the quantity of data recorded by the thermal camera (two hundred 640 × 120 pixel images, 150 kB in size every second or 1.8 GB per minute), we opted for a simple, yet-effective algorithm to extract particle parameters. A first step is to remove the static objects of the image, this being the static background, i.e. a set of components from the image prior to the event. The static background can usually be removed by pre-processing approaches, as reviewed in Brutzer et al. [2011]. Given the time of the beginning of the event ($t = 0$), the easiest way to remove the static background is to consider the difference between the current frame I_t and a reference frame acquired before the event, termed the "background image", $I_{t<0}$ or I_{Ref}. Once the static background was removed, we focused on the moving part of the video. The positions of the particles on the images were detected by subtracting the previous frame I_{t-1} from the current frame I_t. However, all moving elements are detected by this process, including those we did not want to detect (e.g., birds, insects). This is termed the "dynamic background". To solve for this, a first differentiated image at time t (T_t) is generated,

$$T_t = I_t - \frac{\alpha I_{t-1} + \gamma I_{Ref}}{\alpha + \gamma} \; \forall \, t \in \{1, n\} \tag{1}$$

where α and γ are weights derived empirically which change according to the predominance of the static versus dynamic background, those being not independent. In the image, only particles and a low intensity hint of the background persist. Because we only want to detect components among the brightest features, we process $F_t = T_t \cdot \mathbb{1}_{\{I_t - I_0 \geq th\}}$ using a New White Top-Hat transform [Bai and Zhou, 2010]:

$$MNWTH = f - min(((f \oplus \Delta B) \ominus B_b), f) \tag{2}$$

where $\oplus$ is the dilation operator and $\ominus$ the erosion operator. Parameters ΔB and B_b are both square-shaped structuring elements. We apply a 21 pixel diameter

box with, following Bai and Zhou [2010], a three-pixel wide perimeter for ΔB. That is, pixels in the central 15-pixel-wide box have values of zero, and the three-pixel-wide perimeter have values of one.

The second part of the algorithm tracks each particle through time. This allows us to compute the velocity of each particle but also to clean up false detections which may have been occurred during the segmentation process, these being those without matching positions. We chose the maximum intensity pixel of the target as the initial position with subpixel accuracy following Shindler et al. [2010]. Now, $\omega_{i,t} = (x_{i,t}, y_{i,t})$ is the subpixel-position of particle i at time t. We defined the velocity of the particle in the image plane by the pixel distance traveled by the particle between two consecutive frames separated by time t:

$$U_{i,t} = \frac{\|\omega_{i,t+1} - \omega_{i,t}\|}{(t+1) - t}; \tag{3}$$

The position of particle i at time $t + 1$ can now be estimated following several conditions (spatial, intensity, trajectory). We then estimated the velocity in meters per second assuming a planar projection. We also used the radius of the short axis r_S and the radius of the long axis r_L to compute the width of the particle i as an average radius $r = \frac{r_S + r_L}{2}$. The volume (V_i) is then computed assuming a prolate spheroid, so that $V_i = (4/3)\pi r_S^2 r_L$. Finally, given an appropriate density, particle volume can be converted to mass m_i. This algorithm was tested and validated on an artificial experiment (Bombrun et al. [2014]).

1.2 Natural case

The algorithm was tested on videos containing high velocity particles imaged at Stromboli volcano (Aeolian Islands, Italy). In 2012, we completed eight hours of recording spread over four days spanning 27 September-5 October during which time we recorded 13 eruptions. In 2014, we recorded for eight hours on 17 and 18 May, capturing a further 18 events. We set up our high speed camera at Pizzo Sopra la Fossa, a natural platform which overlooks Stromboli's active crater terrace and at a distance of 280 m from the active vent, tilted downwards at an angle of -23 degree. At this distance, we can detect particles down to 5.5 cm.

Emission durations ranged from 5 s to 50 s, with an average of 14. The number of particles ejected during single events detected ranged from 610 to 5 320 with an average of 2 685. A total of 83 220 particles were detected for all 31 eruptions. The particle size distribution reveals that the majority of the particles (67 %) are between the lower limit, 5.5 cm, and 10 cm with a mean particle width of 10 cm and a standard deviation of 5.6 cm. We assess particle shape in terms of the following normalized shape index: $(r_L\text{-}r_S)/(r_L\text{+}r_S)$. Using this index, a perfectly oblate shape will have a value of -1/3 whereas a perfectly prolate shape will have a value of +1/3; a perfect sphere will have a value of 0. We found that only 17 % of our particles approximate a spherical shape. Of the remaining 83 %, 29 % are oblate and 54 % are prolate. The dominance of the prolate shape is consistent with deformation or stretching in the direction of motion.

We used the density of samples, from lapilli to bomb size as collected during campaigns in 2008 [Coló, 2012; Gurioli et al., 2014], 2010 [Gurioli et al., 2013] and 2011 [Leduc et al., 2014] to compute the mass of each particle and the total mass ejected during the eruption. Erupted masses erupted range between 1 270 kg and 11 820 kg with a mean of 4 585 kg. The particle mass distribution revealed that most particles have a low mass, where 46 310 (or 56 %) of all of the detected particles had a mass of less than 4 kg. This population accounts for 10 220 kg or 4.6 % of the total mass. However, the 2 524 particles greater than 25 cm (3 % of the total detected particles) account for 44 % of the total mass. The velocity distribution had a mode between 20 m/s and 30 m/s, with an average velocity of 45 m/s on which the standard deviation was 36 m/s. Particle velocities at Stromboli are generally less than 100 m/s [Chouet et al., 1974; Patrick et al., 2007]. Here, 91 % of all of particles measured had velocities of less than 100 m/s. However, 7 330 particles (8.8 %) had velocities greater than 100 m/s and up to 240 m/s. This approaches the higher velocities recently found for normal explosion at Stromboli by Taddeucci et al. [2012], Delle Donne and Ripepe [2012] and Harris et al. [2012]. Finally, considering the large number of particles detected (83 220), the impact of outliers is vanishingly small. We concluded that our dataset is statistically robust. Full data sets and overview statistics are given in Bombrun et al. [2015].

2 Plume study (meter-sized analysis)

2.1 Target

Our primary objective was to develop an operational algorithm capable of detecting a moving plume through time. A volcanic plume is a mixture of particles, gases, and entrained atmospheric air, which are injected into the atmosphere during a volcanic explosion [Carey and Bursik, 2000]. Thus, the camera used for the plume study was a FLIR Systems SC660. Such volcanic plumes are slow moving targets which may be dispersed on both local and global scales so that frame rates of 1 Hz are more than adequate.

The first step of the algorithm was to consider the differentiation ($D_{t,t-step}$) between the current frame (I_t) and the previous frame (I_{t-step}). We applied a single level discrete 2-D wavelet transformation, using a Daubechies wavelet (db1), on the absolute value of $D_{t,t-1}$. We computed the approximation coefficient matrix to perform a direct reconstruction from the 2-D wavelet coefficient. From the absolute value of the reconstructed image, we computed a single threshold for the image using Otsu's method [Otsu, 1979] to obtained a partial mask of the plume. We cleaned this mask by applying a morphological opening transformation with a 1 pixel radius disk and removing detected elements less than 5 pixels in area. We completed this mask by performing the same process with another differentiation, $D_{t,Ref}$, this being the difference between the current frame (I_t) and a reference frame recorded before the event (I_{Ref}). We summed the two masks to obtain the final differentiated mask. However, because the wavelet transformation was coarse, we needed to redefine the edges. Thus, in the next step, we

performed a morphological reconstruction, i.e., we applied a repeated dilatation process to the mask until its contour fitted the original image, I_t. Each successive dilation was constrained to lie underneath I_t. We cleaned the final image by removing outliers and we computed the contour using a Canny edge detector.

2.2 Applications

We first tested the algorithm on thermal video for the ascent of a volcanic ash plume at Santiaguito volcano, Guatemala. This video was recorded in 2005 and the emission duration is 170 s (i.e. 5 100 frames). The background was composed of a homogeneous sky with weak-intensity meteorological clouds, and the ground contrasts with the plume with a weak-intensity lava flow being apparent on the left side of the vent. Unfortunately the algorithm was too efficient regarding the low contrast image elements so that some meterological clouds were detected as a part of the plume. We removed clouds not pixel-connected with the plume by considering the largest component and improved the contrast by using wavelets on the differentiated image as a pre-processing step.

The second video was recorded at Stromboli volcano, Italy in May the 28^{th} 2012. The camera was set up at Pizzo Sopra la Fossa and pointed at the North-East crater over a direct distance of 300 m so that the image covered a height of 308 m. Plume emission lasted 67 s (i.e. 2 000 frames). The background was a homogeneous sky and cold ground around the vent with another vent on the left which produced unwanted detection. The distance between the camera and the vent was shorter than at Santiaguito, thus the impact of the heat radiated by the crater was more problematic. During plume ascent, the overturn convection continually brought hot spots to the front of the plume creating a random intensity in the plume and making intensity tracking difficult.

The third video was recorded at an experimental facility near Buffalo, USA. The University at Buffalo completed experiments that use small chemical explosive charges buried in layered aggregates to simulate the effects of subsurface hydrothermal and phreatomagmatic explosions [Valentine et al., 2015]. At the same time, three more powerful blasts were performed. These released a plume of fine sand particles. The blast used to test our algorithm was that of Pad 5, Blast 4. The energy produced by the explosion was 2.30×10^6 J and the depth below the surface was 0.5 m. The camera was set up XXXX m from the source so that the field of view was XXXX m height. The ambiant background was composed of trees at ambiant temperature, moving with the wind to create a moving background. The top of the video comprised sky that had a huge contrast with the threes. This video was the most difficult to process due to the numerous and contrasting features in the video. At this point, a global threshold or a double threshold were not solutions anymore.

The last video was recorded at an experimental facility near Munich, Germany, where the Ludwig-Maximilians University completed large-scale ash settling experiments. Natural basaltic ash ($0 - 500$ µm) was released with different controlled volumetric flow rates in a shock tube system. The experiment used to test our algorithm was the #33. The sample came from Monte Rossi Scoria (Italy),

it was fully water saturated, the sample porosity was 30 % and its volume was 29.44 cm^3. The pressure of the decompression was 15 Mpa. The camera was set up horizontally at a distance of 4 m so that the field of view was 4.6 m height.

Conclusion

We present, new approaches to deal with segmentation and feature extraction in thermal video. The first algorithm detects, tracks and parameterizes small dim targets in high-speed IR videos. Based on a mathematical morphology transformation hybridized with refinement by thresholding, this method allowed us to obtain a statistically robust database of 83 000 particles emitted during explosions at Stromboli volcano. Statistically, most of the particles have sizes between 5 and 15 cm, and the majority of individual particle masses are below 0.5 kg. The particle velocity distribution is positively skewed with a mode between 20 and 30 m/s. The second algorithm detected and tracked fine particles in plumes moving across large field of view IR video frames. This method is based on a background subtraction by Daubechies wavelet transformation with a refinement by image reconstruction. It was tested on several cases with different levels of difficulties. We applied it to a volcanic plume in which the heat of the crater restricted the use of a global thresholding and on controlled/experimental explosions in which the background was more complex (moving trees, hot spot created by warm electronic components, etc.). This algorithm proved to be robust enough to detect these plumes despite of the complex image background. These two algorithms are designed to provide necessary information to allow improved understanding and modeling of dynamics during volcanic explosions. Statistically robust databases for vent-leaving particle dynamics remain scarce. Thus, the ability to measure the dynamics of volcanic emissions as they exit the vent and the computation of the particle parameters is an excellent way to understand the dynamics related to the fragmentation and particle emission processes. At the same time, using algorithm output to compute plume parameters such as height, front velocity and spreading angle could be used to constrain models that describe the source geometry and height of volcanic jets [e.g., Jessop and Jellinek, 2014].

Acknowledgments

This research was financed by the French Government Laboratory of Excellence initiative nXXX ANR-10-LABX-0006, the Rgion Auvergne and the European Community.

References

1. Amon, F., and Pearson, C., "Thermal Imaging in Firefighting and Thermography Applications," *Radiometric Temperature Measurements: II. Applications*, vol.43, pp.279–331, 2009.
2. Arora, N., Martins, D., Ruggerio, D., Tousimis, E., Swistel, A.J., Osborne, M.P. and Simmons, R.M., "Effectiveness of a noninvasive digital infrared thermal imaging system in the detection of breast cancer," *The American Journal of Surgery*, vol.196, no.4, pp.523–526, 2008.
3. Bai, X. and Zhou, F., "Analysis of new top-hat transformation and the application for infrared dim small target detection," *Pattern Recognition*, vol.43, no.6, pp.2145–2156, 2010.
4. Bombrun, M., Barra V., and Harris, A., "Algorithm for particle detection and parameterization in high-frame-rate thermal video," *Journal of Applied Remote Sensing*, vol.8, no.1, pp.083549–083549, 2014.
5. Bombrun, M., Harris, A., Barra, V., Gurioli, L., Battaglia, J., and Ripepe, M., "Anatomy of a strombolian eruption: inferences from particle data recorded with thermal video," *Journal of Geophysical Research*, **in prep.**
6. S. Brutzer, B. Hoferlin, and G. Heidemann, "Evaluation of background subtraction techniques for video surveillance," *Computer Vision and Pattern Recognition (CVPR), 2011 IEEE Conference on*, pp.1937–1944, 2011
7. Fernández-Caballero, A., Castillo, J. C., Serrano-Cuerda, J. and Maldonado-Bascón, S., "Real-time human segmentation in infrared videos," *Expert Systems with Applications*, vol.38, no.3, pp.2577–2584, 2011
8. Carey, S., and Bursik., M. (2000). Volcanic plumes. *Encyclopedia of volcanoes. Academic Press, San Diego*. 527–544p.
9. Chouet, B., Hamisevicz, N., and McGetchin, T. R., "Photoballistics of volcanic jet activity at Stromboli," *Journal of Geophysical Research* vol.79, no.32, pp. 4961–4976, 1974.
10. Coló, L., "Study of vesiculation in basalt magma through volcanological, textural and geophysical analyses: The case study of Stromboli," *PhD dissertation, Department of Earth Sciences, Univ. Firenze, Florence, Italy.*
11. Dehn, J., Harris, A. and Ripepe, M., "Infrared Imaging of Strombolian Eruptions," *AGU Fall Meeting Abstracts*, vol.1, pp.C1, 2001.
12. Delle Donne, D., and Ripepe M., "High-frame rate thermal imagery of Strombolian explosions: Implications for explosive and infrasonic source dynamics," *Journal of Geophysical Research* vol.117, no.B9, 2012
13. Faust, O., Acharya, U. R., Ng, E. Y. K., Hong, T. J., and Yu, W., "Application of infrared thermography in computer aided diagnosis," *Infrared Physics & Technology*, vol.66, pp.160-175, 2014.
14. Gurioli, L., Harris, A. J., Coló, L., Bernard, J., Favalli, M., Ripepe, M., and Andronico, D., "Classification, landing distribution, and associated flight parameters for a bomb field emplaced during a single major explosion at Stromboli, Italy," *Geology* vol.41, no.5, pp.559–562, 2013.
15. Gurioli, L., Coló, L., Bollasina, A., Harris, A. J., Whittington, A., and Ripepe, M., "Dynamics of Strombolian explosions: Inferences from field and laboratory studies of erupted bombs from Stromboli volcano," *Journal of Geophysical Research* vol.119, no.1, pp.319–345, 2014.
16. Harris, A. J., Ripepe, M., and Hughes, E. A., "Detailed analysis of particle launch velocities, size distributions and gas densities during normal explosions at Stromboli," *Journal of Volcanology and Geothermal Research*, vol.231, pp.109–131, 2012

17. Harris, A. (2013). *Thermal Remote Sensing of Active Volcanoes: A User's Manual.* Cambridge, UK: Cambridge University Press, 736p.
18. Holst, G. C. (2000). *Common Sense Approach to Thermal Imaging.* Winter Park (FL): JCD Publishing, 377p.
19. Jaggar, T.A., "Volcanologic investigations at Kilauea," *American Journal of Science*, vol.44, pp.161–221, 1917a.
20. Jaggar, T.A., "Thermal gradient of Kilauea lava lake," *Journal of the Washington Academy of Sciences*, vol.7, no.3, pp.397–405, 1917b.
21. de Jong, A. N., "IRST and its perspective," *SPIE's 1995 International Symposium on Optical Science, Engineering, and Instrumentation.* International Society for Optics and Photonics, September 1995. pp.206–213.
22. Kylili, A., Fokaides, P. A., Christou, P., and Kalogirou, S. A., "Infrared thermography (IRT) applications for building diagnostics: A review," *Applied Energy*, vol.134, pp.531-549, 2014.
23. Leduc, L., Gurioli, L., Harris, A., Coló, L., and Rose-Koga, E. F., "Types and mechanisms of strombolian explosions: characterization of a gas-dominated explosion at Stromboli," *Bulletin of volcanology*, 2014.
24. Li, B., Chellappa, R., Zheng, Q., Der, S., Nasrabadi, N., Chan, L., and Wang, L., "Experimental evaluation of FLIR ATR approaches – A comparative study," *Computer Vision and image understanding*, vol.84, no.1, pp.5–24, 2001.
25. Otsu, Nobuyuki, "A Threshold Selection Method from Gray-Level Histograms," *Systems, Man and Cybernetics, IEEE Transactions on*, vol.9, no.1, pp.62–66, Jan 1979.
26. Patrick, M. R., Harris, A. J., Ripepe, M., Dehn, J., Rothery, D. A., and Calvari, S., "Strombolian explosive styles and source conditions: insights from thermal (FLIR) video," *Bulletin of volcanology* vol.69, no.7, pp.769–784, 2007.
27. Shindler, L., Moroni, M., and Cenedese, A., "Spatialtemporal improvements of a two-frame particle-tracking algorithm," *Measurement Science and Technology*, vol.21, no.11, pp.115401, 2010.
28. Shimozuru, D., "Observation of volcanic eruption by an infrared radiation meter," *Nature*, vol.234, pp.457–459, 1971.
29. Spampinato, L., Calvari, S., Oppenheimer, C. and Boschi, E., "Volcano surveillance using infrared cameras," *Earth-Science Reviews* vol.106, no.1, pp.63–91, 2011.
30. Taddeucci, J., Scarlato, P., Capponi, A., Del Bello, E., Cimarelli, C., Palladino, D., and Kueppers, U., "High-speed imaging of Strombolian explosions: The ejection velocity of pyroclasts," *Geophysical Research Letters*, vol.39, no.2, 2012.
31. Tazieff, H., "New investigations on eruptive gases," *Bulletin of Volcanology*, vol.34, no.2, pp.421–438, 1970.
32. Turner, J. S., "The starting plume in neutral surroundings," *Journal of Fluid Mechanics* vol.13, no.3, pp.356–368, July 1962.
33. Valade, S. A., Harris, A. J. L., and Cerminara, M., "Plume Ascent Tracker: Interactive Matlab software for analysis of ascending plumes in image data," *Computers & Geosciences*, vol.66, pp.132–144, 2014.
34. Valentine, G., Graettinger, A.H., Macorps, E., Ross, P., White, J.D.L, Döhring, E., and Sonder, I., "Experiments with vertically- and laterally-migrating subsurface explosions with applications to the geology of phreatomagmatic and hydrothermal explosion craters and diatremes," *Systems, Man and Cybernetics, IEEE Transactions on*, **in prep.**.
35. Yilmaz, A., Shafique, K., and Shah, M., "Target tracking in airborne forward looking infrared imagery," *Image and Vision Computing*, vol.21, no.7, pp.623–635, 2003.

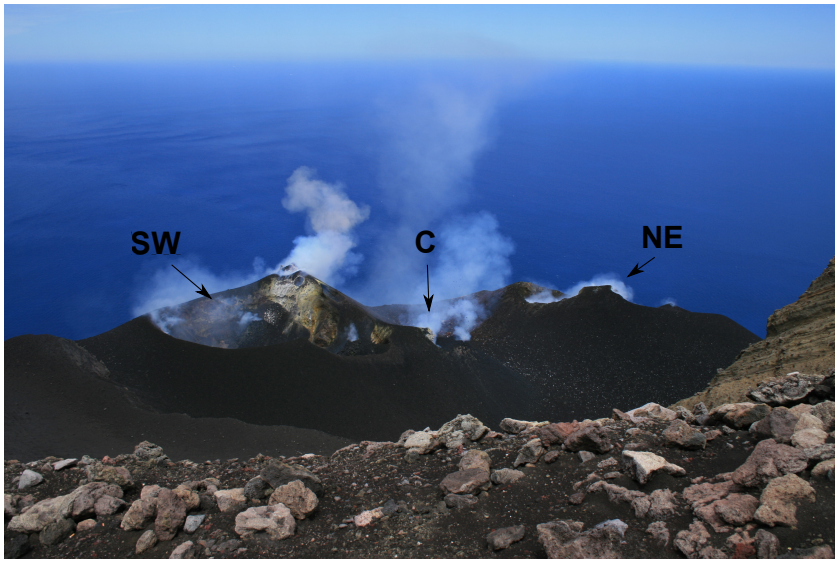

Fig. 1: Overview of the three main craters at Stromboli from Pizzo Sopra la Fossa where the cameras were set up.

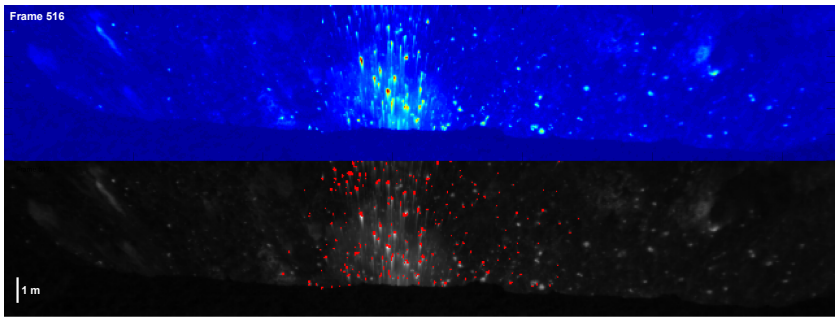

Fig. 2: XX

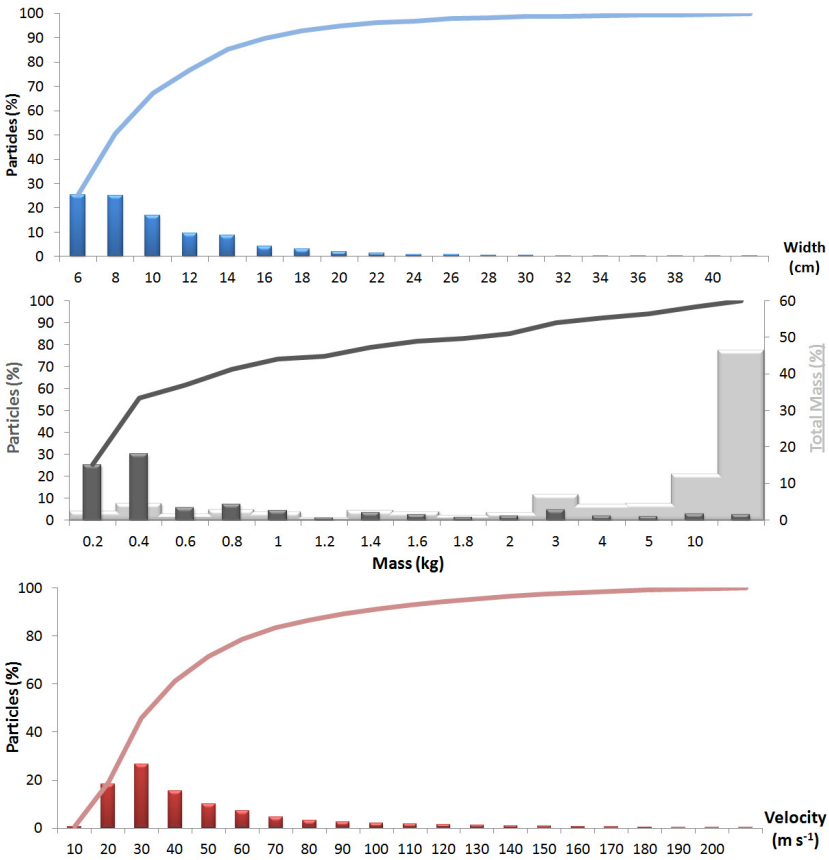

Fig. 3: XX

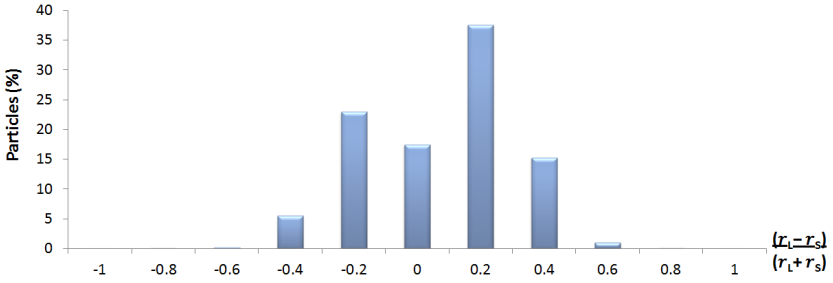
Particles (%)
40
35
30
25
20
15
10
5
0
-1
-0.8
-0.6
-0.4
-0.2
0
0.2
0.4
0.6
0.8
1
$\frac{(r_L - r_S)}{(r_L + r_S)}$

Fig. 4: XX

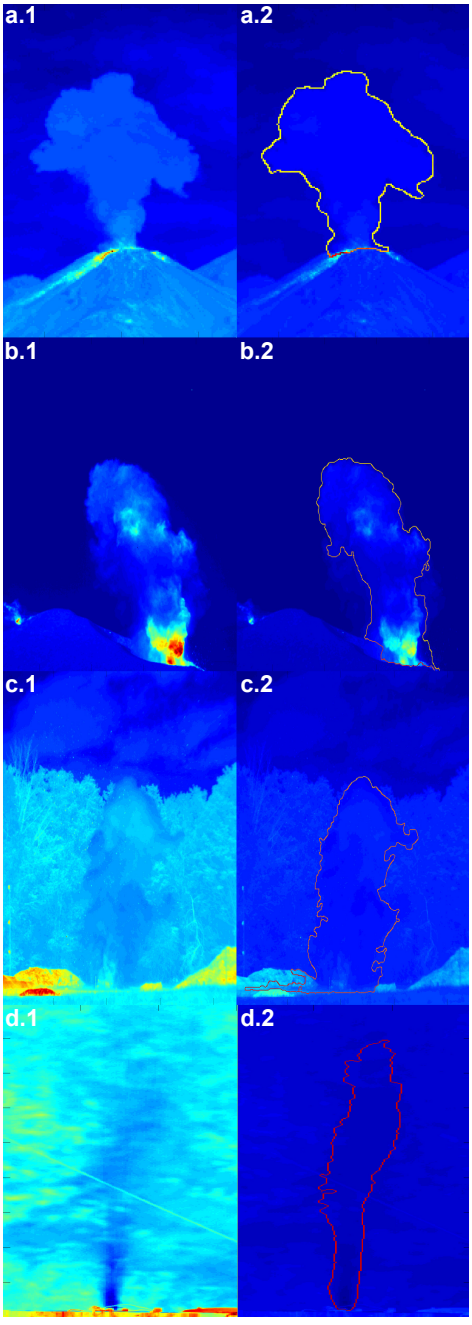

Fig. 5: XX